Infinite-dimensional optimization applied to pair creation from the vacuum

J. Unger,[1] S. Dong,[1,2] R. Flores,[1] Q. Su,[1] and R. Grobe[1]

[1]*Intense Laser Physics Theory Unit and Department of Physics, Illinois State University, Normal, Illinois 61790-4560, USA*

[2]*Key Laboratory for Laser Plasmas, School of Physics and Astronomy, Collaborative Innovation Center of IFSA, Shanghai Jiao Tong University, Shanghai 200240, China*

(Received 1 October 2018; published 27 February 2019)

We examine the electron-positron pair-creation process from the vacuum for general time-dependent external fields. By applying the framework of optimal control theory, we determine those temporal pulse shapes, which can maximize the final number of created positrons for a given set of momenta. In the perturbative regime of sufficiently small pulse energies or short interaction times, we obtain analytical forms that match the computational data of the optimal fields for the chosen sets of positronic momenta.

DOI: 10.1103/PhysRevA.99.022128

I. INTRODUCTION

The subject of electron-positron pair creation from the quantum vacuum state triggered by strong electromagnetic fields has become a widely studied research area. Since the early pioneering works by Heisenberg and Euler [1], Sauter [2], Hund [3], and Schwinger [4], there have been countless articles published that examine the fundamental dynamical features manifest in the spatial and momentum distributions and the total yield for a wide variety of space- and time-dependent electromagnetic field configurations. As this is an intensively studied area, there are also numerous reviews available [5,6]. However, only recently, some first works have been reported that aim to examine how one can possibly tailor the temporal [7–9] or spatial [10] dependence of the external field with the goal to maximize the number of created particles [7–10] after the interaction. This limited number of investigations is surprising, as similar types of optimization questions have been studied routinely for quite a while in many areas of engineering and science [11–18]. For example, in atomic and molecular physics [19–24], the goal is to tailor laser-pulse shapes to control the final outcome of complex chemical reactions or to create or break a particular bond in a molecule or atom. Also, recent experiments have exploited rather sophisticated adaptive laser-pulse-shaping techniques including closed-loop learning algorithms that also permit the independent shaping of the laser's polarization [22] and amplitude, as well as phase.

In the context of the quantum field theoretical pair creation, the recent works of Kohlfürst *et al.* [7,8] and Hebenstreit and Fillion-Gourdeau [9] have suggested that the powerful framework of optimal control theory could be employed to determine the time dependence of the optimal electromagnetic field configuration that leads to the largest number of created electron-positron pairs. Due to the enormous requirements on CPU time, all studies so far in this research have focused on a finite-dimensional optimization, where typically a few phases, amplitudes, or spatial length scales [10] were optimized. While these studies have contributed significantly to open up this research area, the search was naturally confined to optimize only two or three parameters that therefore characterize only a rather restricted space of possible electric fields.

In order to examine the optimization problem from a more fundamental perspective, we aim in this work to explore the space of more general functional forms for the external field. This leads to a computationally much more difficult *infinite-dimensional* optimization problem, where the sole constraint on permitted pulse shapes is provided by fixing their energy. Also, the time dependence of the particle yield has to be consistent with the electron-positron field operator that has to satisfy the Dirac equation.

The main purpose of this work is threefold. First, it suggests that it is computationally feasible to apply an infinite-dimensional optimal control theory to pair creation. Second, we show that the time dependence for the optimum pulse shapes that maximize the positron yield with a given range of momenta can be approximated by simple analytical expressions with remarkable accuracy. Third, part of this work was also motived by a recent article [25], where a superposition principle for the simultaneous optimization (SPSO) for collective responses of sets of classical oscillatorlike systems was introduced [26]. We suggest that this principle is also applicable to the pair-creation dynamics. We find that the particular field that optimizes the total final yield for positrons with a chosen set of momenta can be related directly to a simple linear superposition of those fields, which maximize the positron yield for a specific momentum separately. We show that the corresponding expansion coefficients can be obtained from an eigenvalue problem.

This work is structured as follows. In Sec. II, we introduce the model and its notation, and review how the pair-creation dynamics in spatially homogeneous fields can be mapped onto mutually decoupled sets of two-level-like equations, each describing the positron yield for a given momentum. In Sec. III, we introduce four different optimization schemes and examine the optimal fields in the perturbative (analytical) and nonperturbative regime. In Sec. IV, we examine how the particular type of constraint on the field affects the optimal field. In Sec. V, we derive analytical expressions for the optimal field that lead to a global maximum of the total pair-creation

yield for a given set of positrons' momenta. In Sec. VI, we justify the validity of these expressions by comparing their predictions with the computationally obtained optimal fields for a concrete situation. We finish this article in Sec. VII with a summary and an outlook into future challenges.

II. THE MODEL SYSTEM

If the electric field does not have a spatial inhomogeneity, then the pair-creation dynamics can be described in the temporal gauge by a time-dependent vector potential $A(t)$. In one spatial dimension and in atomic units, the Dirac Hamiltonian takes the form [27,28]

$$H = c\sigma_1[P - qA(t)/c] + c^2\sigma_3, \tag{2.1}$$

where we assume the coupling to a positron with charge $q = +1$. Here, P is the momentum operator, and σ_1 and σ_3 denote the 2×2 Pauli matrices.

In this work, we will use as a basis set the eigenstates of the force-free Hamiltonian, defined as $H_0|p;u\rangle = e_\mathrm{p}|p;u\rangle$ and $H_0|p;d\rangle = -e_\mathrm{p}|p;d\rangle$ with energy $e_\mathrm{p} \equiv [c^4 + c^2p^2]^{1/2}$. For momentum p, the spatial representation of the set is given by the two-component spinors, $\langle x \mid p;u\rangle = N\{[c^2 + e_\mathrm{p}]^{1/2},\ [e_\mathrm{p} - c^2]^{1/2}p/|p|\}\ \exp[ipx]$ and $\langle x \mid p;d\rangle = N\{-[e_\mathrm{p} - c^2]^{1/2},\ [c^2 + e_\mathrm{p}]^{1/2}p/|p|\}\ \exp[ipx]$, where N is the corresponding normalization factor. As the canonical momentum is conserved, i.e., $[P, H] = 0$, the external field $A(t)$ can couple only states with the same momentum $|p;d\rangle$ and $|p;u\rangle$. In other words, the entire pair-creation dynamics is equivalent to the collective dynamics of an infinite set of mutually *independent* two-level systems. We can therefore rewrite H as a sum of independent Hamiltonians over all momenta,

$$\begin{aligned} H \equiv \sum_p [&e_\mathrm{p}|p;u\rangle\langle p;u| - e_\mathrm{p}|p;d\rangle\langle p;d| \\ &- A(t)V_\mathrm{dia} - A(t)V_\mathrm{off}]. \end{aligned} \tag{2.2}$$

Here the on- and off-diagonal couplings are given by

$$\begin{aligned} V_\mathrm{dia}(t) \equiv\ &\langle p;u|\sigma_1|p;u\rangle|p;u\rangle\langle p;u| \\ &+ \langle p;d|\sigma_1|p;d\rangle|p;d\rangle\langle p;d|, \end{aligned} \tag{2.3a}$$

$$\begin{aligned} V_\mathrm{off}(t) \equiv\ &\langle p;d|\sigma_1|p;u\rangle|p;d\rangle\langle p;u| \\ &+ \langle p;u|\sigma_1|p;d\rangle|p;u\rangle\langle p;d|. \end{aligned} \tag{2.3b}$$

Using the functional form of the energy eigenstates from above, the four matrix elements for each p take the form $\langle p;u|\sigma_1|p;u\rangle = cp/e_\mathrm{p} \equiv a_\mathrm{p}$, $\langle p;d|\sigma_1|p;d\rangle = -a_\mathrm{p}$ and $\langle p;d|\sigma_1|p;u\rangle = \langle p;u|\sigma_1|p;d\rangle = c^2/e_\mathrm{p} \equiv b_\mathrm{p}$. For a single momentum p, the state is a superposition of the lower and upper level, $|\Psi_p(t)\rangle = C_\mathrm{p;d}(t)|p;d\rangle + C_\mathrm{p;u}(t)|p;u\rangle$. The time-dependent amplitudes follow from the Dirac equation $i\,\partial|\Psi_p(t)\rangle/\partial t = H|\Psi_p(t)\rangle$ as [29]

$$\begin{aligned} i\,d\,C_\mathrm{p;u}(t)/dt = &[e_\mathrm{p} - A(t)a_\mathrm{p}]C_\mathrm{p;u}(t) \\ &- A(t)b_\mathrm{p}C_\mathrm{p;d}(t), \end{aligned} \tag{2.4a}$$

$$\begin{aligned} i\,d\,C_\mathrm{p;d}(t)/dt = &-A(t)b_\mathrm{p}C_\mathrm{p;u}(t) \\ &- [e_\mathrm{p} - A(t)a_\mathrm{p}]C_\mathrm{p;d}(t). \end{aligned} \tag{2.4b}$$

From a computational perspective, we found it advantageous to convert the complex amplitudes into three real variables, defined as

$$S_1(t) \equiv C_\mathrm{p;d}(t)C_\mathrm{p;u}(t)^* + C_\mathrm{p;d}(t)^*C_\mathrm{p;u}(t), \tag{2.5a}$$

$$S_2(t) \equiv -i[C_\mathrm{p;d}(t)C_\mathrm{p;u}(t)^* - C_\mathrm{p;d}(t)^*C_\mathrm{p;u}(t)], \tag{2.5b}$$

$$S_3(t) \equiv |C_\mathrm{p;u}(t)|^2 - |C_\mathrm{p;d}(t)|^2. \tag{2.5c}$$

This set of Bloch variables [30,31] satisfies the following set of equations:

$$d\,S_1(t)/dt = -2\alpha(t)\,S_2(t), \tag{2.6a}$$

$$d\,S_2(t)/dt = 2\alpha(t)S_1(t) - 2\beta(t)S_3(t), \tag{2.6b}$$

$$d\,S_3(t)/dt = 2\beta(t)S_2(t), \tag{2.6c}$$

where we abbreviated the couplings $\alpha(t) \equiv e_\mathrm{p} - A(t)a_\mathrm{p}$ and $\beta(t) \equiv -A(t)b_\mathrm{p}$. The initial conditions are $S_1(t = 0) = S_2(t = 0) = 0$ and $S_3(t = 0) = -1$. The number density of the created positrons with momentum p is therefore given by $N(p,t) \equiv |C_\mathrm{p;u}(t)|^2 = [1 + S_3(t)]/2$.

III. OPTIMIZATION FOR A SINGLE MOMENTUM

In this section, we examine how we can construct the time dependence of the optimal electric field pulse that can maximize the final number $N(p,T)$ of created positrons for a given momentum p. In order to avoid infinite solutions for $A(t)$, we constrain the time integral of the vector potential to take a finite value $E = \int dt\ A(t)^2$, with the integration limits extending from $t = 0$ to T. Even though E does not correspond to the true electromagnetic energy of the associated electric field (see the more detailed discussion in Sec. IV on this), we denote it below for simplicity as "energy." This means that this optimization problem is relatively universal, as it is characterized by only two given parameters E and T. In the first two appendices, we have summarized the numerical algorithms to determine the optimum pulse shape $A_\mathrm{opt}(t)$ for a given E and T. These algorithms include a predictor-corrector-type (Appendix A), a steepest ascent [32], a Fletcher-Reeves [33], and the Polak-Ribiere [34] based conjugate-gradient method (Appendix B). They differ by computational efficiency, accuracy, as well as their ability to find global maxima and to distinguish between saddle-point solutions and maxima. They require an initial guess for $A(t)$, which is then iteratively improved until the corresponding $N(p,T)$ no longer grows with the number of iterations.

For example, in Fig. 1 we show the final population $N(p,T)$ for $p = 60$ a.u. as a function of the number of iterations for $E = 6000$ and $T = 2 \times 2\pi/(2c^2)$. The time unit $2\pi/(2c^2)$ is suggested by the smallest energy spacing $2c^2$ between the upper and lower energy states with momentum $p = 0$. All four computational schemes used the same temporally constant field $A^{(0)}(t) = (E/T)^{1/2}$ as the initial guess, which generates a low yield of $N(p,T) = 7.96 \times 10^{-4}$. We see that all four methods converge nicely to the maximum $N(p,T) = 0.661$, as indicated by the dashed horizontal reference line. In order to guarantee that the algorithms converge to a global maximum $N(p,T)$, we have varied the choice of the initial guesses for $A(t)$.

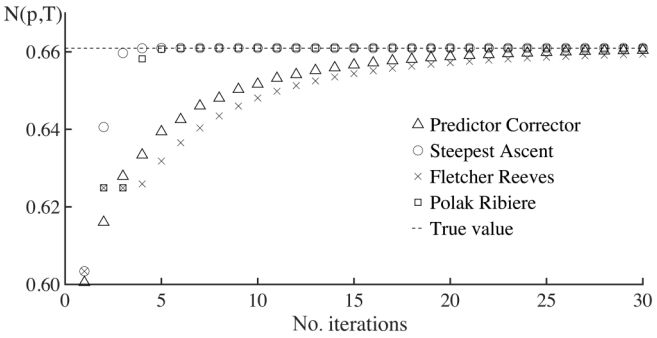

FIG. 1. The final population $N(p,T)$ as a function of the number of iterations for four different computational optimization algorithms. We used the momentum $p = 60$ a.u., and the initial guess $A(t) = (E/T)^{1/2}$. The pulse energy was constrained to $E = 6000$ a.u. and the total interaction time was $T = 2 \times 2\pi/(2c^2)$.

A. The optimal pulses $A_{\rm opt}(t)$ for the perturbative regime

To begin our analytical investigation, we focus first on the perturbative regime, where the field does not have a sufficient time T or energy E to fully excite the upper level. In order to examine which momentum states are easiest to populate under optimal conditions, we have calculated in Fig. 2 the optimum pulse for each p and then graphed the corresponding (largest possible) particle number $N(p,T)$ after the interaction with the (optimal) pulse. Due to the obvious symmetry $p \to -p$, we can focus on positive momenta.

The nearly monotonic decrease of $N(p,T)$ with increasing p shows that it is easiest to create positrons that are at rest. This is consistent with the fact that the off-diagonal coupling elements $-A(t)\,b_{\rm p}$ in Eq. (2.4) fall off monotonically with increasing p. For comparison, we have included in Fig. 2, by the dot-dashed line, the (scaled) squares of the coupling $|b_{\rm p}|^2$. The agreement of $|b_{\rm p}|^2$ with the scaling of the optimal final population $N(p,T)$ with increasing momentum is very good, i.e., $N(p,T) \sim |b_{\rm p}|^2$.

We also note an unexpected oscillatory structure that is superimposed on the decreasing function. This additional structure is related to the changing nature of each optimal field

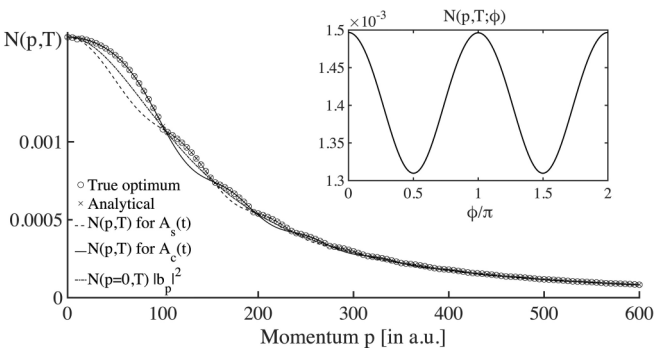

FIG. 2. The largest possible population of the upper level $N(p,T)$ as a function of the momentum (open circles). The continuous and dashed lines are the solutions for two given external fields (3.1a) and (3.1b). For comparison, the dot-dashed line is $0.00167\ |b_{\rm p}|^2$. The pulse energy was constrained to $E = 10$ a.u. and the total interaction time to $T = 2 \times 2\pi/(2c^2)$.

as the momenta increase. It disappears with increasing p and also with increasing interaction time T.

Let us now examine the form of the optimal field $A(t)$ that maximizes $N(p,T)$. Using the framework of optimal control theory (see Appendix A), it is possible in the perturbative regime to derive the following two possible candidates for the optimal field (see Appendix C):

$$A_{\rm C}(t) = A_{0\rm C}\cos[2e_{\rm p}(t - T/2)], \tag{3.1a}$$

$$A_{\rm S}(t) = A_{0\rm S}\sin[2e_{\rm p}(t - T/2)]. \tag{3.1b}$$

Here, $A_{0\rm C} \equiv E^{1/2}[T/2 + \sin(2e_{\rm p}T)/(4e_{\rm p})]^{-1/2}$ and $A_{0\rm S} \equiv E^{1/2}[T/2 - \sin(2e_{\rm p}T)/(4e_{\rm p})]^{-1/2}$ are the corresponding normalization factors for the even and odd functions (with regard to $t = T/2$).

We have accompanied the final populations for the exact (numerically found) optimal fields with the corresponding populations associated with the two given fields of Eqs. (3.1). The superb match indicates that the optimal solutions change back and forth between (3.1a) to (3.1b). For example, for the slowest created positrons ($0 < p < 103$ a.u.), the true optimal field is graphically indistinguishable from the even function given by Eq. (3.1a). For the next band of momenta ($103 < p < 153$ a.u.), the odd function given by Eq. (3.1b) becomes the optimal field, and so on.

As one could have expected, both trigonometric solutions oscillate in time with a frequency $2e_{\rm p}$ that corresponds precisely to the energy difference of the two coupled levels. However, the phase factor corresponding to a shift by $T/2$ is less expected.

Equivalently, one might wonder why for some momenta p the even solution (3.1a) leads to a maximal $N(p,T)$, while other groups of momenta require the odd solution (3.1b). In order to examine several possible physical properties that could determine the phase ϕ for the optimal field, we have computed the $N(p,T)$ for the (energy) normalized function,

$$A(t;\phi) \equiv A_0(\phi)\cos[2e_{\rm p}(t - T/2) + \phi], \tag{3.2}$$

with $A_0(\phi) = E^{1/2}[T/2 + \cos(2\phi)\sin(2e_{\rm p}T)/(4e_{\rm p})]^{-1/2}$. We found that neither the amplitude $A_0(\phi)$ nor the (more physical) energy $\int dt(dA/dt)^2$ can provide the correct criterion. However, we found that for a given momentum, the magnitude of the Fourier component of $A(t,\phi)$ for the resonant frequency $2e_{\rm p}$ is actually largest for the corresponding optimal solution $A_{\rm opt}(t)$. For example, $A(\omega = 2e_{\rm p}, \phi)$ takes a maximum for the phase $\phi = 0$ for $p = 60$, favoring the even solution (3.1a), while for $p = 110$, the amplitude $A(\omega = 2e_{\rm p}, \phi)$ is maximal at $\phi = \pi/2$, thus favoring the odd solution (3.1b).

Obviously, if $2e_{\rm p}T$ is a multiple of π, then $A_0(\phi)$ becomes entirely independent of the phase ϕ, i.e., $A_0(\phi) = E^{1/2}(T/2)^{-1/2}$. This occurs when $p = [\pi^2 n^2/(4T^2) - c^4]^{1/2}/c$, which takes the numerical values $p = 102.777$ (for $n = 5$), $p = 153.211$ (for $n = 6$), and $p = 196.803$ (for $n = 7$). These predictions precisely match the locations of the observed crossing points of the two solutions in Fig. 2.

To examine this interesting relevance of the phase ϕ on the final population of the created positrons, we have graphed in the inset the final population $N(p,T;\phi)$ for $p = 60$ as a function of this phase ϕ. The final population oscillates

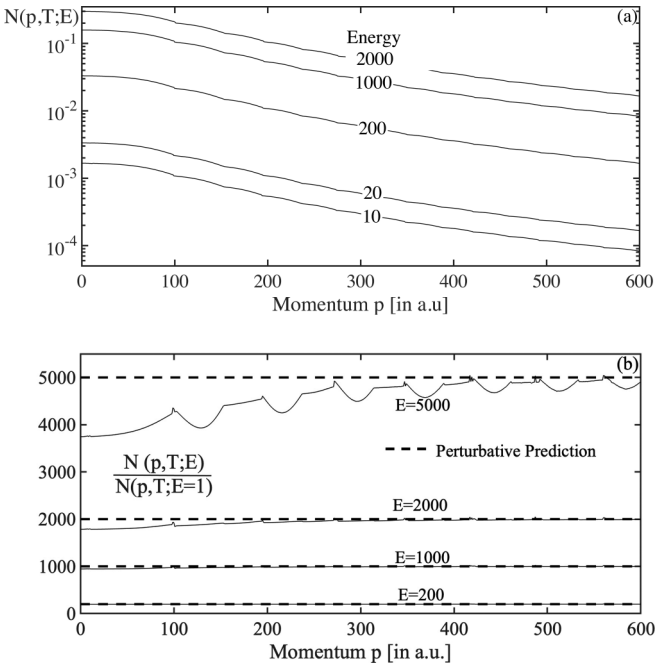

FIG. 3. (a) The final population of the upper level $N(p,T)$ as a function of the momentum for five different pulse energies E. The total interaction time to $T = 2 \times 2\pi/(2c^2)$. (b) The ratio $N(p,T;E)/N(p,T;E = 1\,\text{a.u.})$ as a function of p for the four energies. For comparison, the horizontal dashed lines are the ratios expected from the linear scaling of the perturbative regime.

between $N(p,T) = 1.50 \times 10^{-3}$ for $\phi = 0$ and $\phi = \pi$ and $N(p,T) = 1.31 \times 10^{-3}$ for $\phi = \pi/2$ and $\phi = 3\pi/2$. The fact that the odd solutions ($\phi = \pi/2$ and $\phi = 3\pi/2$) corresponding to Eq. (3.1b) lead to minima in $N(p,T)$ in this one-parameter ($=\phi$) function space does not mean that this field is also a local minimum in the corresponding infinite-dimensional space of all permittable fields $A(t)$. In fact, it corresponds to a saddle point. If we use this particular solution as the initial guess for the predictor-corrector-based numerical optimization scheme, this solution becomes unstable and the consecutive iterations evolve the field $A(t)$ to its global optimum, given by the form (3.1a). However, as the functional gradient of the final population with regard to the field $A(t)$, i.e., $\delta N(p,T)/\delta A(t)$ vanishes at this saddle-point solution, the two gradient-based methods (steepest ascent and conjugate gradient) are less useful as they cannot move the solution away from a saddle point to the true maximum.

B. The transition into the nonperturbative regime

In this section, we probe the nonperturbative domain by increasing the pulse energy E such that the field $A(t)$ can transfer the population completely to the upper level, i.e., $N(p,T) = 1$. In Fig. 3, we show the optimal final population $N(p,T)$ as a function of the positron's momentum p for five different pulse energies E. Generalizing our findings in Sec. III A for $E = 10$, we see that independent of the energy E, it is always easiest to maximize the yield for positrons with a low momentum.

If the energy exceeds about $E = 13\,025$, then the optimal field for $p = 0$ can excite the upper level almost completely,

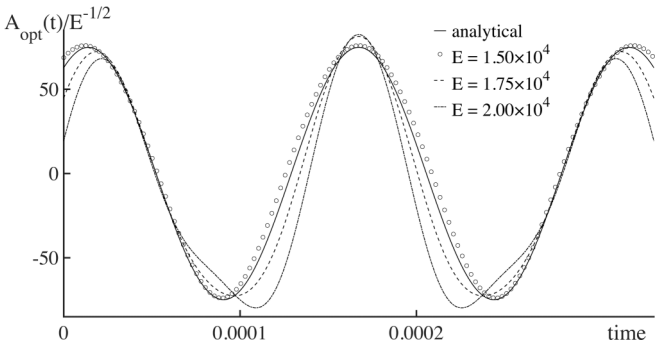

FIG. 4. The optimum field $A_{\text{opt}}(t)$ for three different energies E and momentum $p = 60$. The total interaction time was $T = 2 \times 2\pi/(2c^2)$.

$N(p = 0, T) > 0.99$. In the perturbative low-energy region, the final population depends linearly on the energy E and, as a result, the functions $N(p,T)$ all take the same shape. In order to illustrate this behavior, we have graphed in Fig. 3(b) the ratio $N(p,T;E)/N(p,t;E = 1\,\text{a.u.})$ as a function of p. The constant graphs for small E confirm the linear scaling of the final positron yield with the energy E. For larger E, we see the expected deviations from the linearity, as $N(p,T)$ approaches its maximum possible value of unity. As this upper limit is approached more likely for small p, we see that the nonperturbative corrections occur first for small p as E is increased.

While the change of the scaling of $N(p,T)$ with increasing E suggests a different regime, the corresponding functional form of the optimal field $A_{\text{opt}}(t)$ also deviates from its simple periodic form given by Eq. (3.1a).

In Fig. 4, we show how the optimal pulse begins to differ from Eq. (3.1a) as the energy moves us into the nonperturbative regime. For $E = 1.5 \times 10^4$, the optimum field (circles) is still nearly identical to the perturbative form (continuous graph) even though it can induce a nearly perfect final population of $N(p,T) = 0.9952$. For $E = 2 \times 10^4$, corresponding to $N(p,T) = 0.9999$, we begin to see clear deviations from the simple cosine function as the optimal $A_{\text{opt}}(t)$ takes a rather different shape, which is still even around $t = T/2$.

For even larger energies, we enter an interesting regime in which the search for a unique global maximum $A_{\text{opt}}(t)$ becomes irrelevant. Here there are numerous and rather different functional forms, all of which can excite the final positron yield for a given momentum to the optimal value $N(p,T) > 0.9999$. Here the set of functions $A_{\text{opt}}(t)$ become equivalent to each other, even though (due to their different time dependence) the pathways for $N(p,T)$ to approach unity [from the initial value $N(p,t = 0) = 0$] can be very different.

IV. IMPACT OF THE ENERGY CONSTRAINT ON THE OPTIMAL FIELD

In this section, we show that the theoretical framework is rather universal in the sense that the basic approach leads to similar conclusions even for different constraints for the external field. In the prior discussion, we have given analytical forms of the optimal field in the class of functions $A(t)$ that satisfy $E = \int dt\, A(t)^2$. This led in the perturbative limit to

the main control given by Eq. (C5), $A(t) = -\lambda_0^{-1} b_p[S_2(t) + \lambda_2(t)]$, which could be solved self-consistently with the solutions given in Eqs. (3.1).

If the constraint is modified to the slightly more physical form where the electric energy is kept invariant, i.e., $E = \int dt (dA/dt)^2$, then the required functional gradient $\delta[\int dt (dA/dt)^2]/\delta A(t)$ becomes equal to $-2d^2A/dt^2$ for variations δA that do not change at the boundaries $t = 0$ and $t = T$. As a result, the main control equation contains the second derivative of the field,

$$d^2A/dt^2 = b_p \lambda_0^{-1}[S_2(t) + \lambda_2(t)]. \tag{4.1}$$

We have shown at the end of Appendix C that the solutions $S_2(t) + \lambda_2(t)$ for *any* external field $A(t)$ are given by the linear superposition of $\cos[2e_p(t - T/2)]$ and $\sin[2e_p(t - T/2)]$, where the specific functional form of $A(t)$ determines only the two expansion coefficients. Therefore, the following ansatz for $A_{\rm opt}(t)$ could be a solution of Eq. (4.1),

$$A_{\rm opt}(t) = c_0 + c_1(t - T/2) + c_2 \cos[2e_p(t - T/2)] + c_3 \sin[2e_p(t - T/2)]. \tag{4.2}$$

Due to the normalization constraint, $E = \int dt [dA/dt]^2$, the three (of the four) coefficients have to satisfy

$$E = c_1^2 T + 2\big(c_2^2 + c_3^2\big)e_p^2 T + 4c_1c_3 \sin(e_pT) - \big(c_2^2 - c_3^2\big)e_p \sin(2e_pT). \tag{4.3}$$

Similarly, as in the derivation in Appendix C, for the particular field $\beta(t) = -b_p A_{\rm opt}(t)$ given by Eq. (4.2), we can solve the corresponding equations (C1) for $S_2(t)$ and (C2) for $\lambda_2(t)$ forward and backward in time, respectively. Then the combined solution [required for Eq. (4.1)] turns out to be

$$S_2(t) + \lambda_2(t) = \{c_0\delta_0 + c_2\delta_2\}\cos[2e_p(t - T/2)] + \{c_1\delta_1 + c_3\delta_3\}\sin[2e_p(t - T/2)], \tag{4.4}$$

where the time-independent coefficients are abbreviated as $\delta_0 \equiv 2\sin(e_pT)/e_p$, $\delta_1 \equiv -[e_pT\ \cos(e_pT) - \sin(e_pT)]/e_p^2$, $\delta_2 \equiv [2e_pT + \sin(e_pT)]/(2e_p)$ and $\delta_3 \equiv [2e_pT - \sin(e_pT)]/(2e_p)$. Using the ansatz of Eq. (4.2), the left-hand side (lhs) of the control equation becomes

$$d^2A/dt^2 = -(2e_p)^2\{c_2 \cos[2e_p(t - T/2)] + c_3 \sin[2e_p(t - T/2)]\}. \tag{4.5}$$

It takes the same functional time dependence as Eq. (4.4). By equating the cofactors of the same trigonometric functions, we can now find the coefficients to satisfy

$$-(2e_p)^2 c_2 = b_p \lambda_0^{-1}(c_0\delta_0 + c_2\delta_2), \tag{4.6a}$$

$$-(2e_p)^2 c_3 = b_p \lambda_0^{-1}(c_1\delta_1 + c_3\delta_3). \tag{4.6b}$$

As a side issue, we note that the original constraint, $E = \int dt\, A(t)^2$, leads immediately to $c_0 = c_1 = 0$ as the right-hand side (rhs) [Eq. (4.4)] does not contain any constant or linear term in time. Furthermore, Eqs. (4.6) (for $c_0 = c_1 = 0$) can only be satisfied simultaneously if $\sin(e_pT) = 0$ (or in the limit $T \to \infty$) because only then we have $\delta_2 = \delta_3$. For $\sin(e_pT) \neq 0$, we have only consistent solutions if either c_2 or c_3 vanishes, corresponding to the either an even or odd solution; see Eqs. (3.1). In this case, the value of the momentum determines which of the two extremal solutions $A(t)$ is just a saddle point or a maximum for $N(p, T)$.

In contrast, due to the additional degrees of freedom, the constraint $E = \int dt [dA/dt]^2$ permits a very wide variety of solutions for $A(t)$ that are extrema, i.e., $\delta J/\delta A = 0$. To learn which numerical values for the parameters c_0, c_1, c_2, and c_3 are permitted, we can use Eqs. (4.6) to formally eliminate two degrees of freedom, given by c_0 and c_1,

$$c_0 = c_2\big(-4\lambda_0 e_p^2 - \delta_2 b_p\big)/(\delta_0 b_p), \tag{4.7a}$$

$$c_1 = c_3\big(-4\lambda_0 e_p^2 - \delta_3 b_p\big)/(\delta_1 b_p). \tag{4.7b}$$

Furthermore, if we insert $c_1 = c_1(c_3, \lambda_0)$ from Eq. (4.7b) into the energy constraint (4.3), we can solve the corresponding quadratic equation for λ_0. It has the two solutions $\lambda_0 = \Lambda_1(c_2, c_3; E)$ and $\lambda_0 = \Lambda_2(c_2, c_3; E)$, whose functional forms are rather complicated, as presented in Appendix D.

In order to have physically meaningful (and noncomplex) expressions, it turns out that the two free parameters $\{c_2, c_3\}$ have to be inside an ellipse, i.e., $(c_2/L_2)^2 + (c_3/L_3)^2 \leqslant 1$, where the two semi-axes are given by

$$L_2 = \big\{E\,T/\big[2e_p^2T^2 - E_pT\ \sin(2e_pT)\big]\big\}^{1/2}, \tag{4.8a}$$

$$L_3 = \big\{E\,T/\big[-2 + 2\cos(2e_pT) + 2e_p^2T^2 + e_pT\ \sin(2e_pT)\big]\big\}^{1/2}. \tag{4.8b}$$

This means that we can now formally eliminate λ_0 by introducing E and finally express two of the four coefficients as complicated functions of the other two, i.e., $c_0 = c_0(c_2, \lambda_0) = c_0[c_2, \Lambda_i(c_2, c_3; E)] \equiv C_0(c_2, c_3; E)$ and $c_1 = c_1(c_2, \lambda_0) = c_1[c_3, \Lambda_i(c_2, c_3; E)] \equiv C_1(c_2, c_3; E)$.

Next, if we insert the particular solution $S_2(c_0, c_1, c_2, c_3; t) = S_2[C_0(c_2, c_3; E), C_1(c_2, c_3; E), c_2, c_3; t]$ into the rhs of Eq. (2.6c), $dS_3(t)/dt = 2\beta(t)S_2(t)$, then we can find $S_3(t)$. This gives us the desired form for the optimal $N(p, T) = [1 + S_3(T)]/2$ as a direct function of only the four parameters $(c_2, c_3; E, T)$. Its analytical expression is given by a cumbersome superposition of weighted trigonometric functions with arguments e_pT, $2e_pT$, and $3e_pT$, so we omit its specific form here and give the analytical expression in Appendix D.

However, in Fig. 5, we graph $N(p, T)$ as a function of c_2 and c_3 for $p = 60$ a.u. and $E = 10^9$ a.u. based on $\Lambda_1(c_2, c_3; E)$. The corresponding graph based on $\Lambda_2(c_2, c_3; E)$ (not shown) is very similar. In both cases, the final population is largest for $c_2 = \pm 43.64$ and c_3 approaching zero. This corresponds to $c_1 = 8.72 \times 10^4$ and c_0 approaching infinity.

While the perturbative estimation of the four parameters permits unbound final values for $N(p, T)$, which is unphysical, it still can serve as a good guideline for the parameters for the nonperturbative system, where $0 < N(p, T) < 1$. It is obvious that c_0 cannot approach infinity here. For example, we can examine the suggested values $c_3 = 0$, $c_2 = \pm 43.6$, and $c_1 = 8.7 \times 10^4$, which guarantee that the energy is $E = 10^9$ a.u., and still vary c_0. For example, we found more than $N(p, T) > 99\%$ with the choices $c_0 = 3.245 \times 10^4$, 3.99×10^4, and 4.696×10^4. In these cases, the optimal final value is

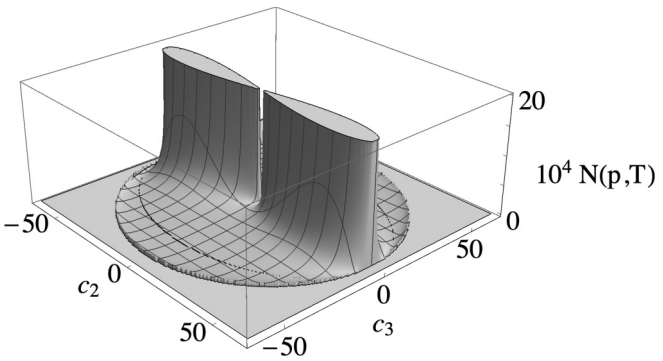

FIG. 5. The final population $N(p,T)$ for the optimum fields $A(t)$ parametrized by the field coefficients c_2 and c_3. [The total interaction time is $2\times 2\pi/(2c^2)$, the pulse energy is $E=10^9$, and the momentum is $p=60$ a.u.; the two semi-axes are $L_2=61.72$ and $L_3=58.08$.]

reached after 4.5, 5.5, and 6.5 cycles of complete population inversions in time, respectively.

V. OPTIMIZATION FOR COLLECTIVE MOMENTUM STATES IN THE PERTURBATIVE LIMIT

In the prior sections, we have seen that for a given pulse energy E and interaction time T, each momentum p leads to its own characteristic optimal field $A_{\rm opt}(t,p)$. It is obvious that a specific field that can optimize the final yield of positrons with lower momenta would not necessarily be the same one that maximizes the yield for more energetic positrons. So the key question in this section is if the information contained in the individual optimal fields $A_{\rm opt}(t,p)$ can be used to predict the functional form of the (single) optimal field that would collectively optimize an entire set of different momenta. The goal is therefore to collectively maximize the total final particle yield, which is given by the sum of the individual yields for each momentum, $\sum_{\rm p}N(p,T)$. If we generalize the framework of optimal control theory derived in Appendix A, the main control given by Eq. (A4) for the optimal field $A(t)$ would take the form

$$A(t)=\lambda_0^{-1}\sum_{\rm p}\{\lambda_1(p)a_{\rm p}S_2(p)+\lambda_2(p)[-a_{\rm p}S_1(p) + b_pS_3(p)]-\lambda_3(p)b_pS_2(p)\}, \tag{5.1}$$

where we have explicitly indicated that the sets of the Lagrange functions $\lambda_i(p)$ as well as the state variables $S_i(p)$ depend on the momentum. This transcendental equation of $A(t)$ simplifies significantly if we again enter the perturbative regime as outlined in Appendix C, leading to

$$A(t)=-\lambda_0^{-1}\sum_{\rm p}b_{\rm p}[S_2(p,t)+\lambda_2(p,t)], \tag{5.2}$$

which is the straightforward generalization of Eq. (C5). In this regime, the equations of motion (C1) and (C2) for the variables $\lambda_2(p,t)$ and $S_2(p,t)$ can be solved analytically in forward and backward time for any source term field $A(t)$, respectively. If we insert these general solutions (containing the integrals over the corresponding Green's functions and the source term) into the rhs of Eq. (5.2), they simplify significantly and the corresponding equation becomes

$$A(t)=\lambda_0^{-1}\int^{\rm T}d\tau\sum_{\rm p}b_{\rm p}^2\cos[2e_{\rm p}(\tau-t)]\,A(\tau). \tag{5.3}$$

This integral equation for the optimal field $A(t)$ is one of the key findings of this work. It is also the generalization for the optimal solutions of Eqs. (3.1) to sets of momenta. In other words, the goal is to construct a specific function $A(t)$ that reproduces itself up to a factor of λ_0 under the action of the linear integral operator $\int^T d\tau\,K(\tau-t)]$, with the kernel $K(t)\equiv\sum_{\rm p}b_{\rm p}^2\cos(2e_{\rm p}t)$. We therefore have to calculate the set of eigenfunctions $A_\mu(t)$ that satisfy $\int^T d\tau\,K(\tau-t)]A_\mu(\tau)=\mu A_\mu(t)$ with the eigenvalues denoted by μ, which then automatically give us the permitted values for the Lagrange multiplier λ_0. The required normalization of the eigenvectors $A_\mu(t)$ to fulfill $E=\int dt\,A_\mu(t)^2$ can be performed at the very end of the calculation.

This computational task can be performed rather easily on a N-dimensional temporal grid, i.e., $t_n\equiv(n-1)\Delta t$ with $\Delta t\equiv T/(N-1)$ and $n=1,2,\ldots,N$. The integral operator is then represented naturally by a $N\times N$ matrix $K_{\rm n,m}=\Delta t\,K(\tau_{\rm n}-t_{\rm m})$, and the resulting eigenvalue problem is given by $\sum_{\rm m}K_{\rm n,m}A_\mu(t_{\rm m})=\mu A_\mu(t_{\rm n})$.

For the special case of a single momentum (as discussed in Sec. III), i.e., $K(t)=b_{\rm p}^2\cos(2e_{\rm p}t)$, it turns out that only two of the N eigenvalues μ of $K_{\rm n,m}$ are nonzero. The two resulting eigenvectors are identical to the solutions proportional to $\cos[2e_{\rm p}(t-T/2)]$ and $\sin[2e_{\rm p}(t-T/2)]$ as derived alternatively in Eqs. (3.1). More generally, for a total number of $P_{\rm tot}$ different momenta, we find exactly $2P_{\rm tot}$ nonzero eigenvalues of $K_{\rm n,m}$.

Alternatively, we can also come to the same conclusion by using the fact that $A(t)$ is real. We therefore have $A(t)=\lambda_0^{-1}\sum_{\rm p}{\rm Re}\{\exp[i2e_{\rm p}(t-T/2)]\int^T d\tau\,b_{\rm p}^2\exp[-i2e_{\rm p}(\tau-T/2)]A(\tau)\}$. If we define the time-independent terms as

$$\chi_{\rm C}\int^T d\tau\,b_{\rm p}^2\cos[2e_{\rm p}(\tau-T/2)]A(\tau), \tag{5.4a}$$

$$\chi_{\rm S}\int^T d\tau\,b_{\rm p}^2\sin[2e_{\rm p}(\tau-T/2)]A(\tau), \tag{5.4b}$$

then this expression for $A(t)$ simplifies and the most general solutions to the integral given by Eq. (5.3) take the simple functional form

$$A_{\rm opt}(t)=\lambda_0^{-1}\sum_{\rm p}\chi_{\rm C}(p)\cos[2e_{\rm p}(t-T/2)] + \chi_{\rm S}(p)\sin[2e_{\rm p}(t-T/2)]. \tag{5.5}$$

This result is quite remarkable. It suggests that the collective optimizing field that simultaneously maximizes the total yield of positrons with many momenta p can be directly related to linear superpositions of the individual optimizing fields $A_{\rm opt}(p,t)$ for each momentum separately. For the special case of two momenta ($P_{\rm tot}=2$), the characteristic weight factors $\chi(p)$ can be constructed analytically, but they are complicated functions of p_1, p_2, E, and T. This remarkable finding is also directly related to the superposition principle for the simultaneous optimization for collective responses (SPSO) that was recently proposed for general dynamical systems [25].

We note that Eq. (5.5) is only the general functional form required for the optimal field, but as the expansion coefficients are still a function of $A(t)$, this is not a concrete solution. That means as a next step, we have to determine the corresponding expansion coefficients χ for a larger number of momenta $P_{\rm tot}$ (up to the overall normalization associated with $\int dt\, A_{\rm opt}^2 = E$). If we insert Eq. (5.5) into Eqs. (5.4), we obtain $\chi_{\rm C}(p) \equiv \lambda_0^{-1}\sum_{\rm q} C_{\rm p,q}\chi_{\rm C}(q)$ and $\chi_{\rm S}(p) \equiv \lambda_0^{-1}\sum_q S_{\rm p,q}\chi_{\rm S}(q)$. This means we can choose the even- and odd-parity manifolds separately from each other. The optimal fields have therefore again a well-defined even- or odd-parity symmetry under reflections around the midpoint $t = T/2$. The expansion coefficients are given by

$$C_{\rm p,q} \equiv \int^T d\tau\, b_{\rm p}^2 \cos[2e_{\rm p}(t - T/2)]\cos[2e_{\rm q}(t - T/2)], \tag{5.6a}$$

$$S_{\rm p,q} \equiv \int^T d\tau\, b_{\rm p}^2 \sin[2e_{\rm p}(t - T/2)]\sin[2e_{\rm q}(t - T/2)], \tag{5.6b}$$

leading to

$$C_{\rm p,q} = b_{\rm p}^2\{\sin[(e_{\rm p} - e_{\rm q})T]/[2(e_{\rm p} - e_{\rm q})] + \sin[(e_{\rm p} + e_{\rm q})T]/[2(e_{\rm p} + e_{\rm q})]\}, \tag{5.7a}$$

$$C_{\rm p,p} = b_{\rm p}^2[2{\rm e}_{\rm p}T + \sin(2e_{\rm p}T)]/(4e_{\rm p}), \tag{5.7b}$$

$$S_{\rm p,q} = b_{\rm p}^2\{\sin[(e_{\rm p} - e_{\rm q})T]/[2(e_{\rm p} - e_{\rm q})] - \sin[(e_{\rm p} + e_{\rm q})T]/[2(e_{\rm p} + e_{\rm q})]\}, \tag{5.7c}$$

$$S_{\rm p,p} = b_p^2[2e_{\rm p}T - \sin(2e_{\rm p}T)]/(4e_{\rm p}). \tag{5.7d}$$

In order to determine the coefficients satisfying $\chi_{\rm C}(p) \equiv \lambda_0^{-1}\sum_{\rm q} C_{\rm p,q}\chi_{\rm C}(q)$ and $\chi_{\rm S}(p) \equiv \lambda_0^{-1}\sum_{\rm q} S_{\rm p,q}\chi_{\rm S}(q)$, we have to diagonalize the corresponding two $P_{\rm tot} \times P_{\rm tot}$ matrices, whose eigenvalues are the permitted values for λ_0. As both $P_{\rm tot} \times P_{\rm tot}$ matrices $C_{\rm p,q}$ and $S_{\rm p,q}$ are real but not symmetric, one could worry that their eigenvalues are not real and merely complex conjugates of each other, which is undesirable. However, the form in Eqs. (5.7) shows that both matrices can be expressed as a product of a (real) diagonal matrix Diag and a real symmetric matrix M, for example, $S_{\rm p,q} = ({\rm Diag}\, M)_{\rm p,q} = \sum_{\rm r} b_{\rm r}^2 d_{\rm p,r} M_{\rm r,q}$. This means that the original eigenvalue problem based on $S_{p,q}$ can be expressed equivalently as a generalized eigenvalue problem based on the Hermitian matrix $M_{\rm r,q}$, i.e., $({\rm Diag}\, M)A_\mu = \mu A_\mu$. By multiplying both sides with ${\rm Diag}^{-1}$, and then multiplying (from the left) with the adjoint eigenvector $A_\mu^\dagger$, we obtain $A_\mu^\dagger M\, A_\mu = \mu A_\mu^\dagger\, {\rm Diag}^{-1} A_\mu$. On the other hand, if we take the adjoint of the original equation, use $M = M^\dagger$ and ${\rm Diag} = {\rm Diag}^\dagger$, and multiply (from the right) with ${\rm Diag}^{-1}A_\mu$, we obtain $A_\mu^\dagger M\, A_\mu = \mu^* A_\mu^\dagger {\rm Diag}^{-1} A_\mu$. Comparing the two expressions shows that the spectrum of $S_{\rm r,q}$ is still real ($\mu = \mu^*$), as desired, despite the lack of the symmetry $S^\dagger = S$.

VI. NUMERICAL EXAMPLE FOR THE OPTIMIZATION FOR COLLECTIVE MOMENTUM STATES

In this section, we will test the validity of this remarkably simple Eq. (5.5) for the optimal field for a set of momenta and also examine the nonperturbative corrections when the pulse energy is large. As the individual optimal fields $A_{\rm opt}(p,t)$ for momenta p that are close to each other are very similar, the resulting collective optimal field $A_{\rm opt}(t)$ associated with the collective response is not too interesting. We therefore illustrate the collective optimizing field for a concrete example, where the momenta are different from each other. In our analytical as well as numerical example, we will construct the global field that maximizes the final yield $\sum_{\rm p} N(p,T)$ summed over the three momenta $p_1 = 1$, $p_2 = 50$, and $p_2 = 100$. We also restrict the interaction time to $T = 20 \times 2\pi/(2c^2)$ and the total pulse energy $E = 1$. The corresponding integration kernel $K(t) = \sum_{\rm p} {b_{\rm p}}^2 \cos(2e_{\rm p}t)$ was represented on a 2000-dimensional temporal grid, and the corresponding 2000×2000 matrix $K_{\rm n,m} = \Delta t\, K(\tau_{\rm n} - t_{\rm m})$ was diagonalized numerically. As pointed out earlier, only 6 out of the 2000 eigenvalues were nonzero, leading to the set of nonvanishing eigenvalues given by $\{1.93,\ 1.90,\ 1.28,\ 1.26,\ 1.06,\ 1.05\} \times 10^{-3}$.

In order to examine the three-dimensional subspace spanned by the nonvanishing even (cosine) solutions [compare Eq. (5.5) above], we have diagonalized the corresponding 3×3 matrix $C_{\rm p,q}$, where the matrix elements are given by Eqs. (5.7a) and (5.7b). Consistent with the prior finding based on the temporal basis states, here we find the three eigenvalues $\{1.93,\ 1.26,\ 1.05\} \times 10^{-3}$ associated with the three eigenvectors $\{0.806, -0.580, 0.121\}$, $\{0.646, 0.735, -0.204\}$, and $\{0.0441, 0.321, 0.946\}$, respectively.

According to Eq. (5.5), the first eigenvector corresponds to the even superposition $A_{\rm opt}(t) = {\lambda_0}^{-1}\sum_{\rm p}\chi_{\rm C}(p)\cos[2e_{\rm p}(t - T/2)]$ with the three coefficients $\chi_{\rm C}(p_1) = 0.806$, $\chi_{\rm C}(p_2) = -0.580$, and $\chi_{\rm C}(p_3) = 0.121$, where ${\lambda_0}^{-1}$ was chosen such that $\int dt A_{\rm opt}(t)^2 = E$. We have determined numerically that it corresponds to a final yield $\sum_{\rm p} N(p,T) = 1.926 \times 10^{-3}$, while the second and third eigenvector leads to $\sum_{\rm p} N(p,T) = 1.263 \times 10^{-3}$ and $\sum_{\rm p} N(p,T) = 1.054 \times 10^{-3}$, respectively. The relative ranking of the magnitudes of the three yields could have been guessed from the three weight factors $\chi_{\rm C}(p_i)$ for each eigenvector. As ${b_{\rm p1}}^2 > {b_{\rm p2}}^2 > {b_{\rm p3}}^2$, the momentum state with p_1 is the most important one. It can contribute with the largest population $N(p_1,T)$ to the combined yield $\sum_{\rm p} N(p,T)$; see also Fig. 2. Therefore, it is not surprising that the first eigenvector [for which $\chi_{\rm C}(p_1) = 0.806$ is largest] leads to the largest yield. As the three corresponding final yields associated with the three eigenvectors of the odd (sine-based) submanifold are all less than 1.926×10^{-3}, we conclude that the superposition based on the first eigenvector $\chi_{\rm C}(p_i)$ is the global maximum of the system.

As an independent test, we have also performed the numerical optimization based on the algorithms discussed in Sec. III. For simplicity, we started the numerical iteration with an initial guess for the field $A(t) = {\rm const}$, which is, of course, far from optimal as it leads to a final yield of only $\sum_{\rm p} N(p,T) = 5.818 \times 10^{-7}$. However, after only 12 iterations (based on the steepest ascent method), the field $A(t)$ has evolved to one that leads to $\sum_{\rm p} N(p,T) = 1.926 \times 10^{-3}$, fully consistent with our theoretical prediction based on perturbation theory.

For comparison, we present in Fig. 6(a) the analytical prediction for the optimal field $A_{\rm opt}(t)$, based on the linear superposition of the three cosine functions and including the energy normalization, which fixes the value of λ_0. We see that

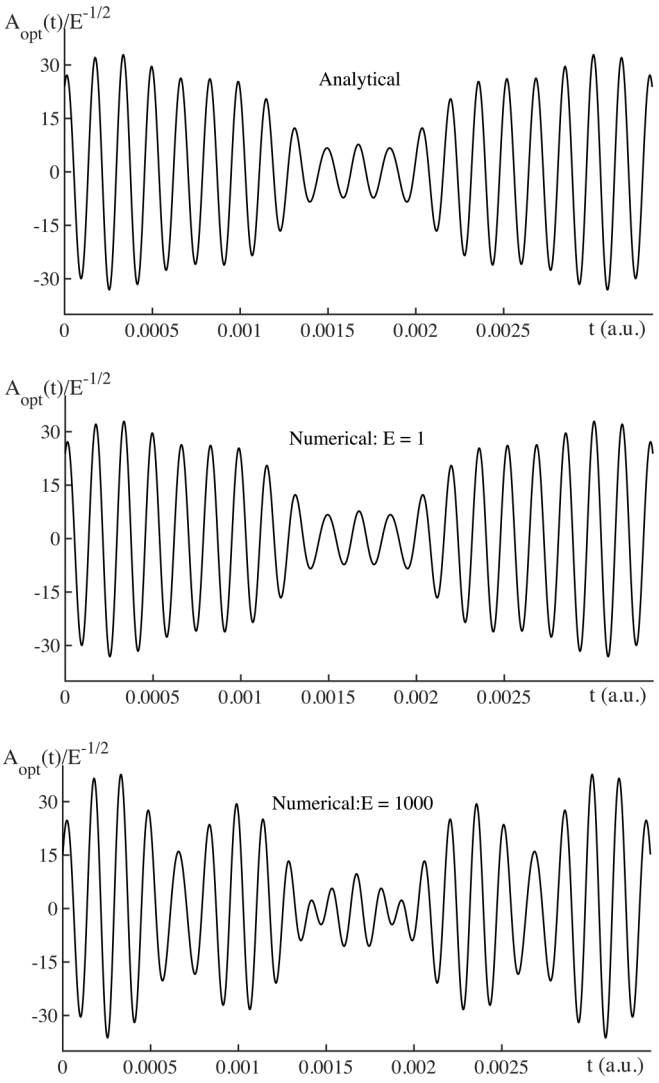

FIG. 6. The optimum field $A_{\rm opt}(t)$ that maximizes the combined total yield for positrons with momenta $p_1 = 1$, $p_2 = 50$, and $p_3 = 100$ a.u. for a total interaction time $T = 20 \times 2\pi/(2c^2)$ and pulse energy E. (a) The analytical prediction according to Eq. (5.5) for $E = 1$. (b) The computationally obtained global optimal field based on the steepest ascent method, using an initial field $A(t) = \text{const}$ and $E = 1$. (c) The nonperturbative optimum field obtained computationally for a larger field energy $E = 1000$.

due to the particular numerical values of the three coefficients, $\chi_C(p_i)$, the resulting optimal form is remarkably different from the three underlying cosinelike functions $A_{\rm opt}(p_1, t)$, $A_{\rm opt}(p_2, t)$, and $A_{\rm opt}(p_3, t)$. For comparison, we graph in Fig. 6(b) the computationally obtained optimum field, based on the infinite-dimensional optimization. The two graphs are indistinguishable from each other.

In order to show how corrections due to nonperturbative effects affect the optimum yield, we have repeated the numerical optimization but increased the field energy E to 1000. This leads to an optimal yield of $\sum_{\rm p} N(p, T) = 1.436$, which is clearly in the nonperturbative regime as the linear energy scaling of the yield based on perturbation theory (see Fig. 3) would predict $\sum_{\rm p} N(p, T) = 1.926$. In Fig. 6(c), we show the corresponding global optimum field $A_{\rm opt}(t)$, which is different from the perturbative prediction.

VII. SUMMARY AND OPEN QUESTIONS

This work illustrates how infinite-dimensional optimization schemes can be applied to the quantum field theoretical problem of maximizing the final particle yield for the strong-field-induced pair-creation process. One of the main purposes was to suggest that the application of optimal control theory in the perturbative limit permits us to derive analytical expressions for the temporal pulse shapes for the optimal field for positrons with a given single momentum as well as for entire sets of momenta. In order to scan through a space of permissible fields $A(t)$ that is as large as possible, we have tried to minimize the number of restrictions on $A(t)$, choosing the simple constraint $E = \int dt\, A(t)^2$ [or $E = \int dt (dA/dt)^2$ in Sec. IV]. As a result of these large degrees of freedom, the obtained optimal fields did not necessarily vanish at $t = 0$ or $t = T$, which one might expect for an external physical field that can be realized in a laboratory. In order to examine those fields that vanish at the boundaries, one can either introduce additional constraints using new Lagrange functions or possibly by introducing penalty functions to the functional objective.

As an experimental electromagnetic field with high frequency would also have a spatial dependence, an infinite-dimensional optimization based on the control theory has not reached the desired stage yet, where it can provide a direct guidance for practical laser field configurations. This is in contrast to atomic, molecular, and optical physics, where related theoretical techniques were substantial to provide quantitative guidance with regard to temporal laser profiles.

Another purpose of the work was to illustrate the recently predicted [25] superposition principle for the simultaneous optimization (SPSO) for a quantum field theoretical system. Quite remarkably, in the perturbative limit of this system, the optimal field that simultaneously optimizes the collective response of several two-level systems $[\sum_{\rm p} N(p, T)]$ can be constructed from a suitable linear superposition of the individual optimal fields $A_{\rm opt}(p, t)$ that maximize the yield for each momentum separately. We showed that the corresponding expansion coefficients for each $A_{\rm opt}(p, t)$ can be obtained from the eigenvectors of a real but asymmetric finite-dimensional matrix. We expect that this superposition principle might also generalize if the spatial inhomogeneity of the fields is included, but obviously more studies are required.

Our numerical analysis was simplified by the fact that spatially homogeneous fields preserve the total momentum such that the dynamics can be described by a set of mutually decoupled two-level systems. To lowest order, small spatial inhomogeneities would couple these sets of equations. One could use this feature to possibly generalize the infinite-dimensional optimization schemes to include the more general function space of space-time-dependent fields.

This article focuses on the optimization of the time dependence of an electric field. For more realistic laser arrangements, the corresponding magnetic field components need to be included as well. In an earlier work [35], it was suggested

that the pair-creation process can be seriously reduced or even brought to a complete halt if an additional (and independent) spatially localized magnetic field accompanies the supercritical electric field. In contrast to the present work, however, both external fields were independent of time and the suppression was associated with the emergence of (static) electrically dressed Landau levels. Furthermore, in order to observe a significant pair suppression for this configuration, a much larger magnetic field was required than the one naturally associated with an electromagnetic laser pulse. Therefore, the effect of the associated (in our present work neglected) magnetic field component of the oscillatory electric field with regard to the suppression mechanism should be negligible. In fact, the correction to the pair-creation process due to the laser's magnetic field component can even enhance the pair-creation rate for some parameters. The interplay between the dynamical effect of the two field components of electromagnetic spatially localized field is certainly very interesting and deserves future investigations.

ACKNOWLEDGMENTS

S.D. and R.F. would like to thank ILP for the nice hospitality during their visits to Illinois State University. We acknowledge helpful discussions with Professors F. Akman and Professor C. Kohlfürst. R.F. acknowledges the support by the exchange program of Illinois State University and ITESM of Mexico. S.D. acknowledges the China Scholarship Council program. This work has been supported by the NSF, NSFC (Grants No. 11529402 and No. 11721091), and the Research Corporation.

APPENDIX A: OPTIMAL CONTROL THEORY BASED ON THE PREDICTOR-CORRECTOR METHOD

For notational simplicity, here we maximize $S_3(T)$, which is, of course, equivalent to maximizing the number density $N(p,T)=[1+S_3(T)]/2$. The predictor-corrector scheme relies on the fact that most constrained optimization problems can be converted to an unconstrained system if Lagrange functions are introduced. As defined in Eqs. (2.5), our dynamical variables [given by the three-component vector $\mathbf{S}(t)\equiv(S_1,S_2,S_3)$] have to fulfill the constraints (state equations) given by Eqs. (2.6), i.e., $d\mathbf{S}/dt=\mathbf{B}[\mathbf{S}(t),A(t)]$ with the initial condition $\mathbf{S}(t=0)=(0,0,-1)$. In order to account for this constraint, we can introduce the three Lagrange functions $\boldsymbol{\lambda}(t)\equiv(\lambda_1,\lambda_2,\lambda_3)$ (called co-states) and the multiplier λ_0 to account for the energy constraint. This leads to the objective J to be extremalized,

$$J=S_3(T)+\lambda_0\left[E-\int dt\,A(t)^2\right]+\int dt\,\boldsymbol{\lambda}\cdot(\mathbf{B}-d\mathbf{S}/dt). \tag{A1}$$

We should note here that due to the linear dependence of J on the Lagrange functions, the field that maximizes $S_3(T)$ does not necessarily maximize J, but leads to a saddle point in J. As it is difficult to develop search algorithms that converge to saddle points, the direct application of standard optimization methods for J is nontrivial. The theoretical analysis and its notation can be simplified if we define a "Hamiltonian" $H\equiv\boldsymbol{\lambda}\cdot\mathbf{B}$. If we compute the functional variation of the objective δJ, we obtain

$$\delta J=\delta S_3(T)+\delta\lambda_0\left[E-\int dt\,A(t)^2\right]-\lambda_0\int dt\,2A\delta A - \int dt[\delta\boldsymbol{\lambda}\cdot d\mathbf{S}/dt+\boldsymbol{\lambda}\cdot\delta[d\mathbf{S}/dt]+\int dt\,\delta H, \tag{A2}$$

where $\delta H=(\partial H/\partial A)\delta A+(\partial H/\partial\mathbf{S})\cdot\delta\mathbf{S}+(\partial H/\partial\boldsymbol{\lambda})\cdot\delta\boldsymbol{\lambda}$. We can apply integration by parts for the terms containing $\delta[d\mathbf{S}/dt]$ using the boundary $\delta\mathbf{S}(t=0)=0$. For the specific definition of H, the partial derivatives simplify to $\partial H/\partial\boldsymbol{\lambda}=\mathbf{B}$. For the optimal solution, we require that the variation δJ is zero, which means the cofactor of each variation, δA, $\delta\lambda_0$, $\delta\boldsymbol{\lambda}$, $\delta\mathbf{S}$, and $\delta\mathbf{S}(T)$, has to vanish, i.e., we require

$$-\lambda_0\,2\mathrm{A}+\partial H/\partial A=0, \tag{A3a}$$

$$E-\int_0^T dtA(t)^2=0, \tag{A3b}$$

$$d\mathbf{S}/dt=\partial H/\partial\boldsymbol{\lambda}=\mathbf{B}\quad\text{with}\quad\mathbf{S}(0)=(0,0,-1), \tag{A3c}$$

$$d\boldsymbol{\lambda}/dt=-\partial H/\partial\mathbf{S}=-\boldsymbol{\lambda}\cdot\partial\mathbf{B}/\partial\mathbf{S}\quad\text{with}\quad\boldsymbol{\lambda}(T)=(0,0,1). \tag{A3d}$$

Equation (A3a) is the main control equation and can be solved formally for $A(t)$ leading to $A(t)=(2\lambda_0)^{-1}\partial H/\partial A$. In the general case, this is a transcendental equation that any candidate for the optimal field $A(t)$ has to satisfy. Using Eq. (2.6), this amounts to

$$\begin{aligned}A(t)&=(2\lambda_0)^{-1}\,\boldsymbol{\lambda}\cdot\partial\mathbf{B}(\mathbf{S},A)/\partial A\\&=\lambda_0{}^{-1}[-\lambda_1\,\partial\alpha/\partial A\,\mathrm{S}_2+\lambda_2(\partial a/\partial A\,S_1-\partial\beta/\partial A\,S_3)\\&\quad+\lambda_3\partial\beta/\partial A\,S_2]\\&=\lambda_0{}^{-1}[\lambda_1 a_\mathrm{p}S_2+\lambda_2(-a_\mathrm{p}S_1+b_\mathrm{p}S_3)-\lambda_3 b_\mathrm{p}S_2].\end{aligned} \tag{A4}$$

In the predictor-corrector scheme, we start with an initial guess for $A(t)$, denoted by $A^{(0)}(t)$ [with $E=\int dt\,A^{(0)}(t)^2$] for which the state and co-state Eqs. (A3c) and (A3d) are solved to compute $\mathbf{S}(t)$ and $\boldsymbol{\lambda}(t)$. We found that the usual Runge-Kutta fourth-order algorithm [32] with about 2000–10 000 temporal step sizes was sufficient. As this particular integration scheme, which iteratively evolves the solutions from $\mathbf{S}(t_\mathrm{n})$ to $\mathbf{S}(t_{\mathrm{n}+1})$ [and $\boldsymbol{\lambda}(t_{\mathrm{n}+1})$ to $\boldsymbol{\lambda}(t_\mathrm{n})$], requires the evaluation of the generator of the differential equations at intermediate times, the field $A(t)$ had to be represented on a finer temporal grid with the double number of grid points.

If we insert these two numerical solutions $\mathbf{S}(t)$ and $\boldsymbol{\lambda}(t)$ into the rhs of the main control given by Eq. (A4), the resulting time-dependent function (lhs) is then interpreted as a "corrected prediction," which we denote by $A^{(1)}(t)$. This field is then used as an improved guess to solve the state and co-state equations again until the difference between $A^{(\mathrm{n})}(t)$ and $A^{(\mathrm{n}+1)}(t)$ is less than a desired numerical tolerance. We should mention that the Lagrange multiplier λ_0 can be obtained easily at each step by requiring the square of the rhs of (A4) to be normalized to E. The chosen sign of λ_0 depends on the specific parameters being studied. Interestingly, the

incorrect choice of this sign manifests itself in the occurrence of unphysical two- (or higher) cycle fixed point solutions, such as $A^{(n)}(t) = A^{(2n)}(t)$, instead of the desired optimum solution $A^{(n)}(t) = A^{(n+1)}(t)$. This iterative predictor-corrector scheme converges nicely in the perturbative regime, but fails to work if the final population $S_3(T)$ approaches unity.

APPENDIX B: GRADIENT-BASED SCHEMES

The parameter regimes where the iterative predictor-corrector scheme converges is unfortunately rather limited. In order to access a wider range of parameters E and T, it is necessary to employ search algorithms that can approach local or (hopefully) global maxima more systematically. The group of algorithms suitable for our dynamics scans through the entire infinite-dimensional function space of permitted functions $A(t)$ by computing an initial search direction $D^{(0)}(t)$ associated with an initial guess $A^{(0)}(t)$ and then performing a one-dimensional line search $J = J[A^{(0)}(t) + \kappa D^{(0)}(t)]$ to find a maximum along this line. In order to restrict the search to only those input fields $A^{(0)}(t) + \kappa D^{(0)}(t)$ that satisfy the energy constraint given by Eq. (A3b), we have energy renormalized each field for each search parameter κ. This step generalizes this commonly used scheme to a "curved line" search. To find κ we first tested the usual golden-ratio-based bisection technique, but found that one has to be careful not to exclude a true global maximum along this curved line and not to settle into a local maximum instead. Overall, the gradient-based algorithms usually converged nicely after a few iterations, after which the search parameter κ turns to zero. Depending on the specific method to determine the search direction for each step, we have compared the predictions of three techniques: the usual steepest ascent technique where the search direction is identical to the functional gradient (Appendices B1 and B2) and the more sophisticated conjugate-gradient-based Fletcher-Reeves and Polak-Ribiere techniques (Appendices B3 and B4). All of these approaches require the determination of the functional derivative $\delta S_3(T)/\delta A(t)$ for a given $A(t)$.

1. Brute-force approach to compute $\delta S_3(T)/\delta A(t)$

Rather than employing any sophisticated strategy to computationally simplify the algorithm, this particular approach is based on computing the functional gradient of $S_3(T)$ numerically without any Lagrange parameters or any other simplifications. The function $A(t)$ was discretized at M points on a temporal grid, with $t_m = T(m-1)/(M-1)$ and $m = 1, 2, \ldots, M$, such that the objective $S_3(T)$ becomes a function of M parameters $A(t_m) \equiv A_m$. For simplicity, we denote the resulting M-dimensional vector $(A_1, A_2, ..., A_M) \equiv \{A_m\}$. This means that the number $S_3(T)$ depends on the entire set of all M parameters $\{A_m\}$, denoted by $S_3(T, \{A_m\})$. The required functional gradient $\delta S_3(T)/\delta A$ is a function of time and therefore represented on the same temporal grid by another M-component vector. The jth component of this gradient vector, denoted by $\delta S_3(T)/\delta A(t_j)$, represents the partial derivative of $S_3(T)$ with regard to a small variation of the field $A(t)$ at particular time t_j. This means we can approximate the functional gradient $\delta S_3(T)/\delta A(t_j)$ by the partial derivative $\partial S_3(T)/\partial A(t_j)$ divided by the grid spacing $\Delta t = T/(M-1)$. This partial derivative can be obtained by using the symmetric three-point finite-difference formula [32],

$$\partial S_3(T)/\partial A(t_j) = [S_3(T, \{A_m + \Delta\, \delta_{m,j})\} - S_3(T, \{A_m - \Delta\, \delta_{m,j})\})]/(2\Delta) + O(\Delta^2), \tag{B1}$$

where $\delta_{m,j}$ denotes the usual Kronecker-delta symbol ($\delta_{m,j} = 1$ if $j = m$ and $\delta_{m,j} = 0$ otherwise) and Δ is a small variation in A_j. We should note that this evaluation of the M components requires, unfortunately, a significant amount of CPU time, as for each set $\{A_m + \Delta\, \delta_{m,j})\}$ (with $j = 1, 2, \ldots, M$) the differential equations (A3c) have to be solved to determine $S_3(T)$ from $S_3(t = 0)$. Numerically, the variational parameter Δ had to be chosen sufficiently small such that the derivative $\partial S_3(T)/\partial A(t_j)$ became independent of Δ. On the other hand, Δ had to be chosen sufficiently large to avoid round-off errors due to subtractive cancellation. We found that Δ in the wide range $10^{-2} < \Delta < 10^{-5}$ was more than sufficient to satisfy both conditions.

In order to avoid any confusion, we should stress again that our optimization problem does not require us to find $A(t)$ such that $\delta S_3(T)/\delta A(t) = 0$. This equation would be true only if the field was unconstrained. The goal is to find the largest $\delta S_3(T)$ only based on those fields $A(t)$ that satisfy the energy constraint. For the desired optimal field, we will have $\delta S_3(T)/\delta A(t) \neq 0$ in general.

2. Approximate but analytical approach to compute $\delta S_3(T)/\delta A(t)$

The direct brute-force approach to calculate the required functional gradient $\delta S_3(T)/\delta A(t)$ is computationally very involved. However, we can invoke the formalism of optimal control theory based on the auxiliary functional $J' \equiv S_3(T) + \int dt[\boldsymbol{\lambda} \cdot (\mathbf{B} - d\mathbf{S}/dt)$. This involves significantly less computational effort, as it will require only the solution to the state and co-state equation for a given $A(t)$. For these specific solutions $\mathbf{S}(t)$ and $\boldsymbol{\lambda}(t)$, the integrand vanishes and we naturally have $J = S_3(T)$, such that the desired gradient $\delta S_3(T)/\delta A(t)$ is identical to $\delta J'/\delta A(t)$. The calculation of $\delta J'/\delta A(t)$ is possible, if we assume first that the four arguments of the functional $J' = J'[S_3(T), \boldsymbol{\lambda}(t), \mathbf{S}(t), A(t)]$ are completely independent of each other, i.e., $\delta S_3(T)/\delta A = \delta \mathbf{S}/\delta A = \delta \boldsymbol{\lambda}/\delta A = 0$, and therefore they are general functions. Under this assumption, the functional derivative can be determined analytically leading to $\delta J'/\delta A(t) = \boldsymbol{\lambda} \cdot \partial \mathbf{B}/\partial A$, as the dependence of $\mathbf{B}$ on A is given by the state equations (2.6). If we then restrict this general expression to the special case that $\boldsymbol{\lambda}(t), \mathbf{S}(t)$ are actual solutions to the state and co-state equations, we naturally obtain the final expression $\delta S_3(T)/\delta A(t) = \boldsymbol{\lambda} \cdot \partial \mathbf{B}/\partial A$. More specifically, we obtain

$$\delta S_3(T)/\delta A(t) = \lambda_1\, a_p S_2 + \lambda_2(-a_p S_1 + b_p S_3) - \lambda_3 b_p S_2. \tag{B2}$$

Except for the energy normalization factor λ_0, this expression is surprisingly identical to the rhs of the main control equation (A4), which was a transcendental equation for $A_{opt}(t)$. This means that the functional gradient $\delta J'/\delta A$, when evaluated at

the state and co-state solutions $\boldsymbol{\lambda}(t)$ and $\mathbf{S}(t)$ for a particular $A(t)$, takes the similar form as the optimum $A_{\mathrm{opt}}(t)$ itself.

3. Steepest ascent and conjugate-gradient technique based on Fletcher-Reeves

For the standard steepest ascent technique, one usually takes the functional gradient evaluated for $A^{(\mathrm{n})}(t)$ as the new search direction, i.e., $D^{(\mathrm{n})}(t) = \partial J/\partial A$. As is well known and thoroughly discussed in the literature [33], this algorithm is characterized [for a (noncurved) line search] by the fact that two consecutive search directions are perpendicular to each other. In some cases, this is problematic and can lead to a very high number of required iterations to achieve convergence to the optimum solution. Also, once the line search parameter κ happens to vanish for one iteration (one particular curved-line search direction), then the whole iteration comes to an end and one can no longer explore other regions in the Hilbert space of possible $A(t)$.

The more sophisticated conjugate-gradient scheme avoids this problem by involving all prior search directions into the new one. There are numerous ways in which this can be accomplished. We have examined the Fletcher-Reeves approach [32], where the new search direction $D^{(\mathrm{n})}(t)$ is a linear superposition of the prior search direction and the direction provided by the gradient associated with $A^{(\mathrm{n})}(t)$, i.e., $D^{(\mathrm{n})}(t) = \partial J/\partial A^{(\mathrm{n})} + \mu^{(\mathrm{n}-1)} D^{(\mathrm{n}-1)}(t)$. Here the expansion coefficient can be computed from the dimensionless ratio $\mu^{(\mathrm{n})} = \int_0^T dt[\partial J/\partial A^{(\mathrm{n})}]^2 / \int_0^T dt[\partial J/\partial A^{(\mathrm{n}-1)}]^2$. This means that any new search direction is different and depends on all prior search directions. It also follows that in contrast to the steepest ascent method, if μ happens to be zero for a particular search direction, the iteration does not necessarily come to a halt as μ can change to a nonzero value again for later iterations.

4. Conjugate-gradient technique based on Polak-Ribiere

Very similar to the Fletcher-Reeves approach, also for the Polak-Ribiere technique [33] is the new search direction $D^{(\mathrm{n})}(t)$ given by a superposition of the prior search direction and the direction provided by the gradient associated with $A^{(\mathrm{n})}(t)$, i.e., $D^{(\mathrm{n})}(t) = \partial J/\partial A^{(\mathrm{n})} + \mu^{(\mathrm{n}-1)} D^{(\mathrm{n}-1)}(t)$. The two methods vary only in the particular way the weight factor $\mu^{(\mathrm{n})}$ associated with $D^{(\mathrm{n})}(t)$ is computed. In the Polak-Ribiere scheme, it is determined as $\mu^{(\mathrm{n})} = \int_0^T dt\, \partial J/\partial A^{(\mathrm{n})}(\partial J/\partial A^{(\mathrm{n})} - \partial J/\partial A^{(\mathrm{n}-1)}) / \int_0^T dt[\partial J/\partial A^{(\mathrm{n}-1)}]^2$, so the gradients of the last two iterations need to be taken into account.

APPENDIX C: THE OPTIMAL PULSE IN THE PERTURBATIVE LIMIT

In this appendix, we will show that both solutions for $A(t)$ given by Eq. (3.1) extremalize the "action" J of Eq. (A1) in the perturbative limit, i.e., they satisfy the main control given by Eq. (A3a). In this limit, the field's energy E (or the time T) is not sufficiently large to fully populate the upper level and both the main control given by Eq. (A4) as well as the state and co-state equations (A3c) and (A3d) can be simplified, which permits analytical solutions.

If we approximate $S_3(t) \approx -1$ in Eq. (2.6b) and assume that the coefficient $\alpha(t) \approx e_{\mathrm{p}}$, the state equations (2.6) simplify to

$$d\,S_1(t)/dt = -2e_{\mathrm{p}} S_2(t), \tag{C1a}$$

$$d\,S_2(t)/dt = 2e_{\mathrm{p}} S_1(t) + 2\beta(t). \tag{C1b}$$

The same argument applies also to the co-state equations (A3d), which take the same form as Eq. (2.6). If we assume that $\lambda_3(t) \approx 1$ the co-state equations become

$$d\lambda_1(t)/dt = -2e_{\mathrm{p}}\lambda_2(t), \tag{C2a}$$

$$d\lambda_2(t)/dt = 2e_{\mathrm{p}}\lambda_1(t) - 2\beta(t). \tag{C2b}$$

For the particular function $\mathrm{A}(t) = A_{0\mathrm{C}} \cos[2e_{\mathrm{p}}(t - T/2)]$, i.e., $\beta(t) = -b_{\mathrm{p}} A(t)$, both sets of equation can be solved, leading to

$$\begin{aligned} S_2(t) = {} & -b_{\mathrm{p}} A_{0\mathrm{C}} \{2e_{\mathrm{p}} t \cos[2e_{\mathrm{p}}(t - T/2)] \\ & + \cos[e_{\mathrm{p}} T] \sin[2e_{\mathrm{p}} t]\}/(2e_{\mathrm{p}}), \end{aligned} \tag{C3a}$$

$$\begin{aligned} \lambda_2(t) = {} & b_{\mathrm{p}} A_{0\mathrm{C}} \{4e_{\mathrm{p}}(t - T)\cos[2e_{\mathrm{p}}(t - T/2)] \\ & + \sin[2e_{\mathrm{p}}(t - 3T/2)] + \sin[2e_{\mathrm{p}}(t - T/2)]\}/(4e_{\mathrm{p}}). \end{aligned} \tag{C3b}$$

As both equations were driven by a force that is in resonance with the system, each solution contains a term that grows linearly in time. However, if we add both solutions (as will be required by the main control equation; see below), this resonant term cancels out, leading to

$$\begin{aligned} S_2(t) + \lambda_2(t) = {} & -b_{\mathrm{p}}[2e_{\mathrm{p}} T + \sin(2e_{\mathrm{p}}\mathrm{T})]/(2e_{\mathrm{p}}) A_{0\mathrm{C}} \\ & \times \cos[2e_{\mathrm{p}}(t - T/2)]. \end{aligned} \tag{C4}$$

In the same perturbative spirit, also the main control equation (A3a), $A = (2\lambda_0)^{-1}\partial H/\partial A$, can be simplified under the same assumptions, leading to

$$\begin{aligned} A &= (2\lambda_0)^{-1}[\lambda_1 \partial B_1/\partial A + \lambda_2 \partial B_2/\partial A + \lambda_3 \partial B_3/\partial A] \\ &\approx (2\lambda_0)^{-1}[-2\lambda_2 b_{\mathrm{p}} - 2\, b_{\mathrm{p}} S_2] \\ &= -b_{\mathrm{p}}\lambda_0{}^{-1}[S_2(t) + \lambda_2(t)]. \end{aligned} \tag{C5}$$

If we insert the expression for $S_2(t) + \lambda_2(t)$ into the rhs and choose the Lagrange parameter λ_0 such that the prefactor $b_{\mathrm{p}}\lambda_0{}^{-1}\, b_{\mathrm{p}}[2e_{\mathrm{p}} T + \sin(2e_{\mathrm{p}} T)]/(2e_{\mathrm{p}}) = 1$, then the right-hand side of (C5) is equal to $A_{0\mathrm{C}}\cos[2e_{\mathrm{p}}(t - T/2)]$. This proves that this particular field $A(t)$ solves the main control equation exactly, which is a necessary condition to extremalize the objective function J. The same sequence of arguments can be applied to prove that $A_{\mathrm{opt}}(t) = A_{0\mathrm{S}} \sin[2e_{\mathrm{p}}(t - T/2)]$ also extremalizes J.

As a next step, we can even find an analytical expression for the largest possible density $N(p, T)$. If we insert the particular solutions into Eq. (2.6c), i.e., $d\,S_3(t)/dt = 2\beta(t) S_2(t)$, then we can obtain the solution

$$\begin{aligned} S_3(t) = {} & [b_{\mathrm{p}} A_{0\mathrm{C}}/(4e_{\mathrm{p}})]^2 \big\{\big(1 + 8{e_{\mathrm{p}}}^2 t^2\big) - \cos(4e_{\mathrm{p}} t) \\ & + 8\, e_{\mathrm{p}}\, t \cos[2e_{\mathrm{p}}(t - T)] \sin(2e_{\mathrm{p}} t)\big\} - 1, \end{aligned} \tag{C6}$$

which for $t = T$ takes a remarkable simple form. We finally obtain for $N(p, T) = [1 + S_3(T)]/2$,

$$N(p, T) = [b_{\mathrm{p}} A_{0\mathrm{C}}/(4e_{\mathrm{p}})]^2 [4e_{\mathrm{p}} T + \sin(2e_{\mathrm{p}}\mathrm{T})]^2. \tag{C7}$$

This is the absolute maximum final number of positrons with momentum p. It is generated by the optimum field $\mathrm{A}(t) = A_{0\mathrm{C}}\cos[2e_\mathrm{p}(t - T/2)]$. The same analysis for the case, where $\mathrm{A}(t) = A_{0\mathrm{S}}\sin[2e_\mathrm{p}(t - T/2)]$ is the optimum field, leads to

$$N(p, T) = [b_\mathrm{p}A_{0\mathrm{S}}/(4e_\mathrm{p})]^2[4e_\mathrm{p}T - \sin(2e_\mathrm{p}T)]^2. \quad \text{(C8)}$$

Both analytical expressions are graphed in Fig. 1.

As a side issue, we should point out that the structure of the solution (C4) is not so unexpected. In fact, it is valid for any functional form of $A(t)$. If we add Eqs. (C1b) and (C2b), the external force $\beta(t)$ cancels out and we we obtain $d(S_2 + \lambda_2)/dt = 2e_\mathrm{p}(S_1 + \lambda_1)$. Similarly, adding Eqs. (C1a) and (C2a) gives us $d(S_1 + \lambda_1)/dt = -2e_\mathrm{p}(S_2 + \lambda_2)$. When we combine them, we see that the resulting equation for $(S_2 + \lambda_2)$ follows that of a simple harmonic oscillator motion, $d^2(S_2 + \lambda_2)/dt^2 = -4{e_\mathrm{p}}^2\ (S_2 + \lambda_2)$. However, the "initial" and "final" conditions for this equation are mixed [$S_2(t = 0) = 0$ and $\lambda_2(t = T) = 1$] and therefore $S_2(t) + \lambda_2(t)$ depends nontrivially on the specific form of the original external field $A(t)$.

APPENDIX D

In this appendix, we summarize the cumbersome analytical expressions for the discussion of Sec. IV. If we insert the expressions for c_0 and c_1 [Eqs. (4.7)] into the energy constraint given by Eq. (4.3), we obtain for the two solutions of the resulting quadratic equation $\lambda_{1,2} = \Lambda_{1,2}(c_2, c_3) = -4c_3(c_3\, z_1 \pm \delta_1 {z_2}^{1/2})/z_3$, where

$$z_1 \equiv \delta_3\, T - 2\,\delta_1 \sin(e_\mathrm{p}T), \quad \text{(D1)}$$

$$z_2 \equiv 2\,{c_3}^2 + E\,T - 2\big({c_2}^2 + {c_3}^2\big)\,{e_\mathrm{p}}^2\,T^2 - 2\,{c_3}^2\cos(2e_\mathrm{p}T) + \big({c_2}^2 - {c_3}^2\big)\,e_\mathrm{p}T\sin(2e_\mathrm{p}T), \quad \text{(D2)}$$

$$z_3 \equiv {\delta_1}^2\big[-E + 2\big({c_2}^2 + {c_3}^2\big)\,{e_\mathrm{p}}^2\,T\big] + {c_3}^2\,T{\delta_3}^2 + \delta_1\big[-4\,{c_3}^2\,\delta_3\sin\big(e_\mathrm{p}\,T\big)\big] + \big({c_3}^2 - {c_2}^2\big)\,e_\mathrm{p}\,\delta_1\sin(2e_\mathrm{p}T). \quad \text{(D3)}$$

If we insert the solution $S_2(t)$ obtained for the parametrized field $A(t) = A(t; c_0, c_1, c_2, c_3)$ into Eq. (2.6c), i.e., $d\,S_3(t)/dt = 2\beta(t)S_2(t)$, then we can solve for $S_3(T)$. When this solution is evaluated at the final time T, it is given by the form

$$S_3(p, T; c_0, c_1, c_2, c_3) = \big(16{e_\mathrm{p}}^6\big)^{-1}[w_0 + w_1\cos(e_\mathrm{p}T) + w_2\cos(2e_\mathrm{p}T) + w_3\cos(3e_\mathrm{p}T) + w_4\cos(4e_\mathrm{p}T) + w_5\sin(e_\mathrm{p}T) + w_6\sin(2e_\mathrm{p}T) + w_7\sin(3e_\mathrm{p}T)], \quad \text{(D4)}$$

with the eight coefficients

$$w_0 \equiv -16\,{e_\mathrm{p}}^6 + c^4\big\{4\,{c_1}^2\big(1 + {e_\mathrm{p}}^2\,T^2\big) + {e_\mathrm{p}}^2\big[16\,{c_0}^2 + \big({c_2}^2 + {c_3}^2\big)\big(1 + 8\,{e_\mathrm{p}}^2\,\mathrm{T}^2\big)\big]\big\}, \quad \text{(D5)}$$

$$w_1 \equiv -4\,e_\mathrm{p}c^4\big[-2c_0c_2e_\mathrm{p} + c_1c_3\big(1 + 4{e_\mathrm{p}}^2\,T^2\big)\big], \quad \text{(D6)}$$

$$w_2 \equiv 4\,c^4\big[-4{c_0}^2{e_\mathrm{p}}^2 + {c_1}^2\big(-1 + {e_\mathrm{p}}^2\,T^2\big)\big], \quad \text{(D7)}$$

$$w_3 \equiv 4\,c^4e_\mathrm{p}(c_1c_3 - 2\,c_0c_2e_\mathrm{p}), \quad \text{(D8)}$$

$$w_4 \equiv -c^4{e_\mathrm{p}}^2\big({c_2}^2 + {c_3}^2\big), \quad \text{(D9)}$$

$$w_5 \equiv 4\,c^4\,{e_\mathrm{p}}^2\,T(5\,c_1\,c_3 + 8\,c_0c_2e_\mathrm{p}), \quad \text{(D10)}$$

$$w_6 \equiv -8\,c^4\,e_\mathrm{p}\,T\,\big[{c_1}^2 + \big({c_3}^2 - {c_2}^2\big){e_\mathrm{p}}^2\big], \quad \text{(D11)}$$

$$w_7 \equiv 4\,c^4{e_\mathrm{p}}^2\,T\,c_1\,c_3. \quad \text{(D12)}$$

[1] W. Heisenberg and H. Euler, Z. Phys. **98**, 714 (1936).
[2] F. Sauter, Z. Phys. **69**, 742 (1931).
[3] F. Hund, Z. Phys. **117**, 1 (1941).
[4] J. S. Schwinger, Phys. Rev. **82**, 664 (1951).
[5] For a comprehensive review, see, e.g., A. Di Piazza, C. Müller, K. Z. Hatsagortsyan, and C. H. Keitel, Rev. Mod. Phys. **84**, 1177 (2012).
[6] For a more recent review, see B. S. Xie, Z. L. Li, and S. Tang, Matter Radiat. Extremes **2**, 225 (2017).
[7] C. Kohlfürst, Master's thesis, Graz University, 2012, arXiv:1212.0880.
[8] C. Kohlfürst, M. Mitter, G. von Winckel, F. Hebenstreit, and R. Alkofer, Phys. Rev. D **88**, 045028 (2013).
[9] F. Hebenstreit and F. Fillion-Gourdeau, Phys. Lett. B **739**, 189 (2014).
[10] S. S. Dong, M. Chen, Q. Su, and R. Grobe, Phys. Rev. A **96**, 032120 (2017).
[11] D. E. Kirk, *Optimal Control Theory: An Introduction* (Prentice-Hall, Englewood Cliffs, NJ, 1970).
[12] R. Dechter, *Constraint Processing* (Morgan Kaufmann, Burlington, 2003).
[13] D. S. Naidu, *Optimal Control Systems* (CRC Press, Baca Raton, FL, 2003).
[14] J. J. Leader, *Numerical Analysis and Scientific Computation* (Addison Wesley, Reading, MA, 2004).
[15] R. Battiti, M. Brunato, and F. Mascia, *Reactive Search and Intelligent Optimization* (Springer-Verlag, Heidelberg, 2008).
[16] W. Sun and Y. X. Yuan, *Optimization Theory and Methods: Nonlinear Programming* (Springer-Verlag, Heidelberg, 2010).
[17] A. Gosavi, *Simulation-Based Optimization* (Springer-Verlag, Heidelberg, 2015).
[18] D. Bertsekas, *Dynamic Programming and Optimal Control* (Athena Scientific, Reston, VA, 2017).
[19] J. Werschnik and E. K.U Gross, J. Phys. B **40**, R175 (2007).
[20] A. G. Butkovskiy and Y. I. Samoilenko, *Control of Quantum Mechanical Processes and Systems* (Kluwer Academic, Dordrecht, 1990).
[21] J. Zabczyk, *Mathematical Control Theory* (Birkhauser, Basel, Switzerland, 1990).
[22] T. Brixner, G. Krampert, T. Pfeifer, R. Selle, G. Gerber, M. Wollenhaupt, O. Graefe, C. Horn, D. Liese, and T. Baumert, Phys. Rev. Lett. **92**, 208301 (2004).

[23] V. Ramakrishna, R. Ober, X. Sun, O. Steuernagel, J. Botina, and H. Rabitz, Phys. Rev. A **61**, 032106 (2000).
[24] S. G. Schirmer, H. Fu, and A. I. Solomon, Phys. Rev. A **63**, 063410 (2001).
[25] S. Dong, R. Flores, J. Unger, Q. Su, and R. Grobe, Phys. Rev. E **98**, 012221 (2018).
[26] For related earlier work on optimization, see, e.g., S. Glasgow, M. Meilstrup, J. Peatross, and M. Ware, Phys. Rev. E **75**, 016616 (2007); S. Glasgow and M. Ware, Phys. Rev. A **80**, 043817 (2009); S. A. Glasgow, J. Corson, and C. Verhaaren, Phys. Rev. E **82**, 011115 (2010).
[27] B. Thaller, *The Dirac Equation* (Springer, Berlin, 1993).
[28] T. Cheng, Q. Su, and R. Grobe, Contemp. Phys. **51**, 315 (2010).
[29] G. R. Mocken, M. Ruf, C. Müller, and C. H. Keitel, Phys. Rev. A **81**, 022122 (2010).
[30] L. Allen and J. H. Eberly, *Optical Resonance and Two-Level Atoms* (Wiley, New York, 1975).
[31] P. Milonni and J. H. Eberly, *Lasers* (Wiley, New York, 1988).
[32] W. H. Press, S. A. Teukolsky, W. T. Vetterlin, and B. P. Flannery, *Numerical Recipes: The Art of Scientific Computing* (Cambridge University Press, New York, 1992).
[33] R. Fletcher and C. M. Reeves, Comp. J. **7**, 149 (1964).
[34] E. Polak and G. Ribière, Rev. Franc. Inf. Recherche Oper. **3**, 35 (1969).
[35] Q. Su, W. Su, Z. Q. Lv, M. Jiang, X. Lu, Z. M. Sheng, and R. Grobe, Phys. Rev. Lett. **109**, 253202 (2012).